catalysts

MDPI

Article

Core-Shell MnO_2-SiO_2 Nanorods for Catalyzing the Removal of Dyes from Water

Wei Gong, Xianling Meng, Xiaohong Tang and Peijun Ji *

Department of Chemical Engineering, Beijing University of Chemical Technology, Beijing 100029, China; gongwei209@126.com (W.G.); xlmengbuct@126.com (X.M.); xhtangbuct@126.com (X.T)

* Correspondence: jipj@mail.buct.edu.cn; Tel.:+86-10-64423254

Academic Editor: Keith Hohn

Received: 23 November 2016; Accepted: 28 December 2016; Published: 6 January 2017

Abstract: This work presented a novel core-shell MnO_2@m-SiO_2 for catalyzing the removal of dyes from wastewater. MnO_2 nanorods were sequentially coated with polydopamine (PDA) and polyethyleneimine (PEI) forming MnO_2@PDA-PEI. By taking advantage of the positively charged amine groups, MnO_2@PDA-PEI was further silicificated, forming MnO_2@PDA-PEI-SiO_2. After calcination, the composite MnO_2@m-SiO_2 was finally obtained. MnO_2 nanorod is the core and mesoporous SiO_2 (m-SiO_2) is the shell. MnO_2@m-SiO_2 has been used to degrade a model dye Rhodamine B (RhB). The shell m-SiO_2 functioned to adsorb/enrich and transfer RhB, and the core MnO_2 nanorods oxidized RhB. Thus, MnO_2@m-SiO_2 combines multiple functions together. Experimental results demonstrated that MnO_2@m-SiO_2 exhibited a much higher efficiency for degradation of RhB than MnO_2. The RhB decoloration and degradation efficiencies were 98.7% and 84.9%, respectively. Consecutive use of MnO_2@m-SiO_2 has demonstrated that MnO_2@m-SiO_2 can be used to catalyze multiple cycles of RhB degradation. After six cycles of reuse of MnO_2@m-SiO_2, the RhB decoloration and degradation efficiencies were 98.2% and 71.1%, respectively.

Keywords: MnO_2 nanorods; polydopamine; dyes; SiO_2

1. Introduction

Dyes are widely used in the textiles, cosmetics, paper, leather, ceramics, and inks industries [1,2]. It is estimated that 15% of the dye is lost during processes and is released in wastewater [2]. Dye pollutants are an important source of environmental contamination and cause significant pollution to groundwater [3]. Dyes are generally resistant to light and moderate oxidative agents. Without proper treatment, these dyes can be stable in the water for a much longer period of time [4].

A number of physical and physicochemical technologies have been developed for the removal of dyes from aqueous solutions, including adsorption techniques [3,4], membrane processes [5,6], and degradation of dyes through oxidation under the assistant of catalysts [7–10]. Various materials have been used as adsorbents for the removal of dyes, such as biocoagulants [1], fruit peels [3], and cellulose-based bioadsorbents [4]. Mesoporous silica materials with a low toxicity have high specific areas and large interior spaces. Dye molecules can be entrapped in silica nanoparticles and films [11–14]. Silica-based materials, carboxylic acid-functionalized silica [15,16], silica-alumina oxide [17], silica hydrogels [18], mesoporous silica [19,20], and carboxymethyl tamarind-g-poly(acrylamide)/silica [21] have been investigated as adsorbents for removing dyes from wastewater. Except for the physical adsorption methods, removing dyes can be accomplished through oxidation, such as electrooxidation [22], photocatalytic degradation [23], and oxidation by graphene oxide nanosheet-based material [24]. Manganese oxides are highly reactive minerals and have oxidation capacities for organic compounds [25]. Because of the relatively low cost and environmental

compatibility, manganese oxides—for example, acid-activated MnO_2 [26], α-MnO_2 nanowires [27], manganese dioxide nanosheets [28], and manganese oxides with hollow nanostructures [29]—have been investigated for oxidative degradation of dyes.

In this work, a novel core-shell catalytic material MnO_2@m-SiO_2 for oxidative degradation of dyes has been developed. Scheme 1 illustrates the preparation route for the composite MnO_2@m-SiO_2. MnO_2 nanorods were first coated with polydopamine to form MnO_2@PDA, and then polyethyleneimine (PEI) was bound to MnO_2@PDA, forming MnO_2@PDA-PEI. Further silicification of this material formed MnO_2@PDA-PEI-SiO_2. After calcination under 400 °C, MnO_2@m-SiO_2 was prepared. This material has been utilized to degrade a model dye Rhodamine B (RhB). The mesoporous m-SiO_2 layer on the surface of the composite adsorbed and enriched RhB; the RhB molecules were transported through the mesoporous m-SiO_2 layer by diffusion, and then the MnO_2 nanorods catalyzed the degradation of RhB.

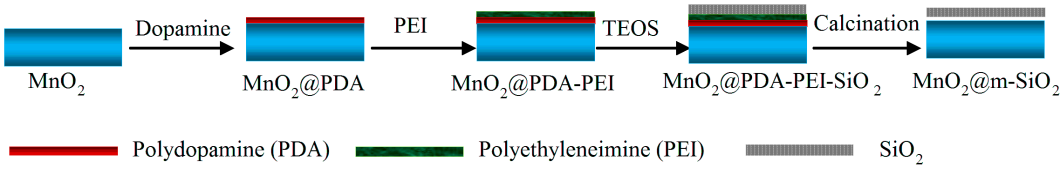

Scheme 1. Schematic illustration of preparation of MnO_2@m-SiO_2.

2. Results and Discussion

2.1. Preparation of MnO_2@m-SiO_2

Scheme 1 illustrates the procedures for the preparation of MnO_2@m-SiO_2. MnO_2 nanorods were coated with a thin film of polydopamine (PDA) to form MnO_2@PDA by impregnating the MnO_2 nanorods in the dopamine solution, in which polymerization of dopamine occurred at an alkaline condition. PDA is one kind of catechol amine. When MnO_2@PDA was added to the polyethyleneimine (PEI) solution, PEI was bound to PDA through Michael addition of amines on the unsaturated indole rings and Schiff base formation reactions between the amines and catechols [30]. Thus, MnO_2@PDA was coated with PEI forming MnO_2@PDA-PEI. The positively charged amine groups on the surface of MnO_2@PDA-PEI provide prerequisites for further silicification [31]. When MnO_2@PDA-PEI was added to the solution of TEOS, electrostatic interactions occurred between the positively charged amine groups of PEI and negatively charged silicic acid resulted from the hydrolysis of the methyl groups of TEOS [31]. Protonated and nonprotonated amine groups of the PEI chains formed hydrogen bonds with the oxygen, facilitating the formation of Si–O–Si bonds. Thus, MnO_2@PDA-PEI was silicificated and MnO_2@PDA-PEI-SiO_2 was formed. The composite MnO_2@m-SiO_2 was obtained after calcination under 400 °C.

In the FTIR spectra, as illustrated in Figure 1, the band centered at 1588 cm^{-1} was assigned to ring C=C and ring C=N stretching modes [32], confirming that MnO_2 was coated with PDA, forming MnO_2@PDA. When PEI was bound to MnO_2@PDA forming MnO_2@PDA-PEI, the band at 1291 cm^{-1} appeared, which was ascribed to the stretching vibration of C–N of primary and secondary amines [33]. The band at 1097 cm^{-1} was ascribed to the vibration of Si–O–Si bonds [34], resulting from the silicification of MnO_2@PDA-PEI. After calcination under 400 °C forming MnO_2@m-SiO_2, the bands at 1605 and 1586 cm^{-1} were significantly reduced, indicating the removal of PEI and PDA after the calcination. As a result, the band at 1097 cm^{-1} became prominent.

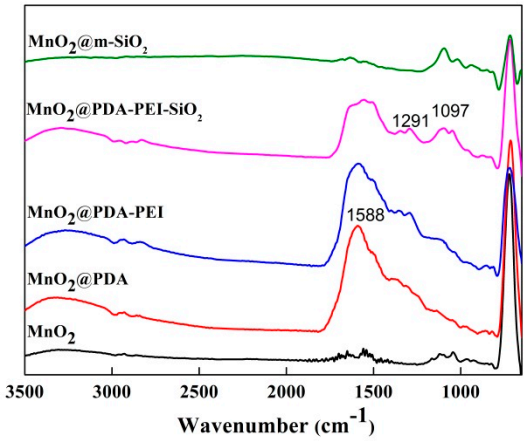

Figure 1. FTIR spectra of MnO_2, MnO_2@PDA, MnO_2@PDA-PEI, MnO_2@PDA-PEI-SiO_2 and MnO_2@m-SiO_2. PDA: polydopamine; PEI: polyethyleneimine

Figure 2 shows the XPS spectra of MnO_2, MnO_2@PDA, MnO_2@PDA-PEI, MnO_2@PDA-PEI-SiO_2, and MnO_2@m-SiO_2. The spectrum of MnO_2@PDA shows that the intensity of oxygen is relatively increased compared to that of MnO_2, and the peaks for carbon and nitrogen appeared. After coating PEI onto MnO_2@PDA, the intensities of carbon and nitrogen were relatively increased. After the silicification of MnO_2@PDA-PEI, the peak intensity of oxygen was relatively increased, and the peaks of Si2s and Si2p appeared. After calcination forming MnO_2@m-SiO_2, the peak intensities of carbon and nitrogen were significantly decreased, indicating that most of the PDA and PEI were removed.

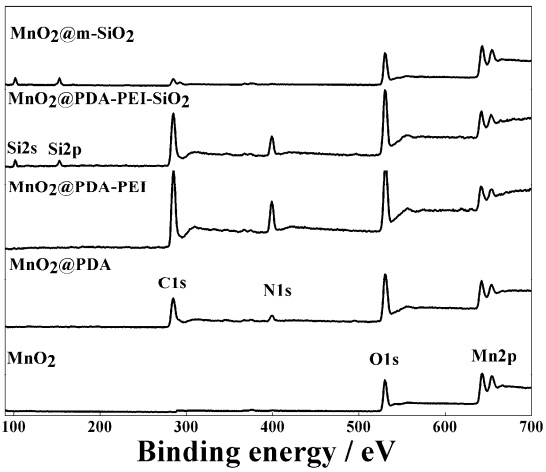

Figure 2. XPS spectra of MnO_2, MnO_2@PDA, MnO_2@PDA-PEI, MnO_2@PDA-PEI-SiO_2 and MnO_2@m-SiO_2.

Figure 3 shows the XPS spectra of Mn 2p3/2 region for MnO_2, MnO_2@PDA, and MnO_2@m-SiO_2. The peaks around 641.4 and 642.4 eV are assigned to Mn^{3+} and Mn^{4+}, respectively [35]. The surface element ratio of Mn^{3+} to Mn^{4+} for MnO_2 was 0.230. After coating PDA on MnO_2, the surface element ratio was increased to 0.72. This is due to the redox reaction between MnO_2 and dompamine. After removing PDA and PEI from MnO_2@PDA-PEI-SiO_2 by calcination under 400 °C, the surface element ratio of Mn^{3+} to Mn^{4+} for MnO_2@m-SiO_2 was 0.232, which is almost equal to that for MnO_2. It is indicated that the oxidation state of Mn of MnO_2@m-SiO_2 has changed little in comparison to that for MnO_2.

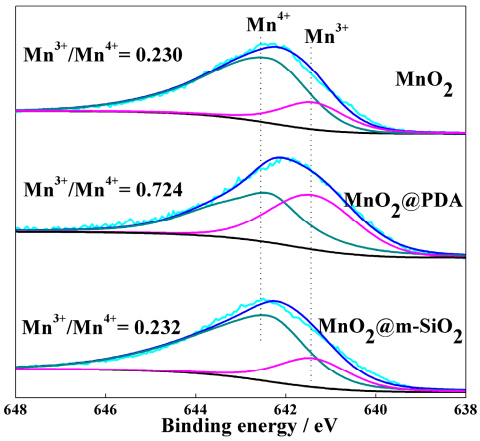

Figure 3. Non-normalized and curve fitted Mn 2p3/2 XPS spectra of MnO_2, MnO_2@PDA, and MnO_2@m-SiO_2.

The nitrogen adsorption–desorption isotherm of MnO_2 and MnO_2@m-SiO_2, and the corresponding Barrete–Joynere–Halenda (BJH) pore size distribution are presented in Figure 4. The isotherm of MnO_2@m-SiO_2 displayed a hysteresis loop within the relative pressure range of 0.5–0.9 (Figure 4a), indicating the presence of mesoporous pores in the sample of MnO_2@m-SiO_2. The pore size distributions of the two samples (Figure 4b) were calculated by desorption isotherm using the Barrete–Joynere–Halenda method [36]. For the sample of MnO_2, there was a small peak around 2.6 nm. For the sample of MnO_2@m-SiO_2, there was a sharp peak around 3.8 nm. On the basis of the N_2 adsorption–desorption isotherms, the BET surface area of MnO_2 and MnO_2@m-SiO_2 were determined to be 33.2 m^2/g and 51.7 m^2/g, respectively. The increase in BET surface area for MnO_2@m-SiO_2 is ascribed to the shell being mesoporous SiO_2. A larger specific surface area of MnO_2@m-SiO_2 is beneficial for adsorbing and removing dyes.

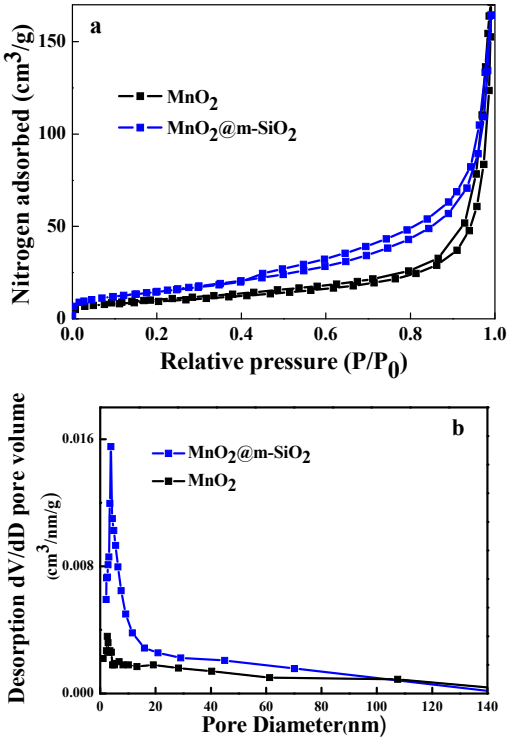

Figure 4. Nitrogen adsorption (**a**) and desorption (**b**) isotherms for MnO_2 and MnO_2@m-SiO_2.

2.2. Catalytic Degradation of RhB with MnO_2@m-SiO_2

The degradation of rhodamine B (RhB) was carried out by immersing MnO_2@m-SiO_2 in the RhB solutions. To have a comparison, MnO_2 and MnO_2@PDA-PEI-SiO_2 were also used for the degradation/removal of RhB. During the processes, three obvious peaks of UV-Vis spectra were monitored at different immersion times of the materials. The peak at 554 nm is due to the presence of C=N and C=O groups of RhB (Figure 5). The peak at 499 nm is due to N-deethylated intermediate products of RhB. The decrease in absorbance at 259 nm is ascribed to the degradation of the aromatic part of RhB [37]. The intensities of the absorbance at 554 and 259 nm were used to calculate the decolorization and degradation efficiencies, respectively.

Concomitant with the UV-Vis spectra, the photographs of decoloration of the RhB solutions are also presented. Thus, the progress of decoloration of RhB can be directly observed. The RhB decoloration efficiencies after 2 min were 98.7%, 64.9%, and 7.0% for MnO_2@m-SiO_2, MnO_2, and MnO_2@PDA-PEI-SiO_2, respectively. These quantitative results are consistent with the decoloration results as illustrated by the upright photographs. When using MnO_2 and MnO_2@m-SiO_2 (Figure 5a,c), the absorbance at 499 nm indicated the formation of N-deethylated intermediate products. This confirmed that both MnO_2 and MnO_2@m-SiO_2 can oxidize RhB. While using MnO_2@PDA-PEI-SiO_2, the absorbance at 499 nm was not observed, indicating that MnO_2@PDA-PEI-SiO_2 could not oxidize RhB, and the decoloration is due to the adsorption of RhB. After 90 min, the RhB degradation efficiencies for MnO_2 and MnO_2@m-SiO_2 were 61.2% and 84.9%, respectively. The results in Figure 5 demonstrated that MnO_2@m-SiO_2 exhibited a much higher efficiency for the degradation of RhB than MnO_2. It has been also demonstrated that MnO_2@PDA-PEI-SiO_2 adsorbed RhB from its aqueous solutions but did not degrade RhB. This is possibly due to fact that the PDA and PEI films have prevented the contacting of RhB with MnO_2.

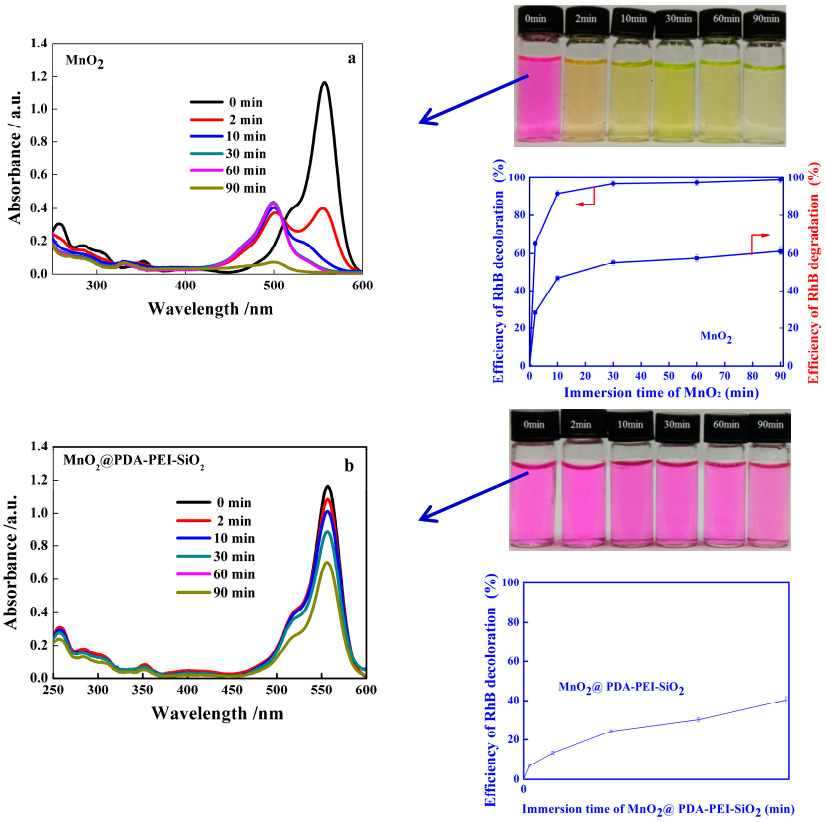

Figure 5. *Cont.*

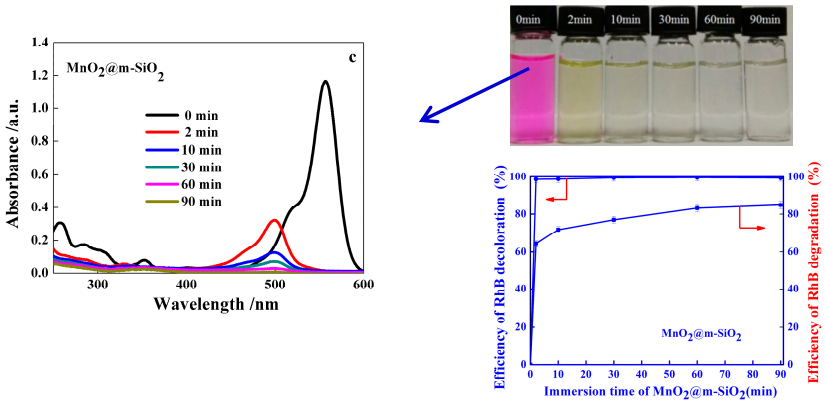

Figure 5. UV-Vis spectra of the rhodamine B solution at different immersion times for MnO_2 (**a**); MnO_2@PDA-PEI-SiO_2 (**b**); and MnO_2@m-SiO_2 (**c**).

The photographs correspond to respective UV-Vis spectra. The figures in blue show the efficiencies of RhB decoloration/degradation. The efficiency of RhB decoloration is defined as $(A_0^{dec} - A_{90}^{dec})/A_0^{dec}$; A_0^{dec} and A_{90}^{dec} are the absorbances of the RhB solutions at 554 nm at initial time and after 90 min, respectively. The efficiency of RhB degradation is defined as $(A_0^{deg} - A_{90}^{deg})/A_0^{deg}$; A_0^{deg} and A_{90}^{deg} are the absorbances of the RhB solutions at 259 nm at the initial time and after 90 min, respectively. The concentrations of MnO_2, MnO_2@PDA-PEI-SiO_2, and MnO_2@m-SiO_2 were 5 mg/mL, and the concentration of RhB was 5 mg/mL.

2.3. Mechanism for Degradation of RhB with MnO_2@m-SiO_2

The TEM images in Figure 6, showing the morphology for MnO_2, MnO_2@PDA-PEI-SiO_2, and MnO_2@m-SiO_2 can help understand the advantages of MnO_2@m-SiO_2 over MnO_2. By sequentially coating PDA and PEI and further silicification, a dense film was clearly observed on MnO_2@PDA-PEI-SiO_2 (Figure 6b). As mentioned above, the film of PDA-PEI-SiO_2 prevented the contacting of RhB with the MnO_2 nanorods. As a result, MnO_2@PDA-PEI-SiO_2 could not degrade RhB. The film of PDA-PEI-SiO_2 became mesoporous SiO_2 by removing the PDA-PEI coatings through calcination under 400 °C. A tiny gap between the MnO_2 core and the mesoporous SiO_2 shell was generated as shown in Figure 6c. Scheme 2 schematically illustrates the processes for the degradation of RhB by using MnO_2@m-SiO_2. RhB molecules were first adsorbed and enriched on the surface of MnO_2@m-SiO_2. Then, the RhB molecules were transferred through the mesoporous SiO_2 (m-SiO_2) into the tiny gap region between m-SiO_2 and MnO_2 nanorods, and were then degraded by the MnO_2 nanorods. The enrichment of RhB was due to the adsorption capability of SiO_2 for dyes [11]. Mesoporous silica has demonstrated being capable of entrapping dye molecules [19]. Herein, the diffusion transfer of RhB through mesoporous SiO_2 (m-SiO_2) was driven by the concentration differential of RhB, as the concentration of RhB inside the tiny gap region was always kept lower due to the continuous degradation of RhB by the MnO_2 nanorods. The composite MnO_2@m-SiO_2 with a core-shell structure combines the multiple functions together, including adsorption/enrichment, transfer and oxidation of RhB. The synergistic effect of the multiple functions facilitated and promoted the degradation of RhB. Thus, MnO_2@m-SiO_2 exhibited a much higher efficiency for degradation of RhB than MnO_2. Figure 7 shows the consecutive use of MnO_2@m-SiO_2 for the degradation of RhB. After six cycles of reuse of MnO_2@m-SiO_2, the RhB decoloration and degradation efficiencies were 98.2% and 71.1%, respectively, indicating a good reusability of MnO_2@m-SiO_2.

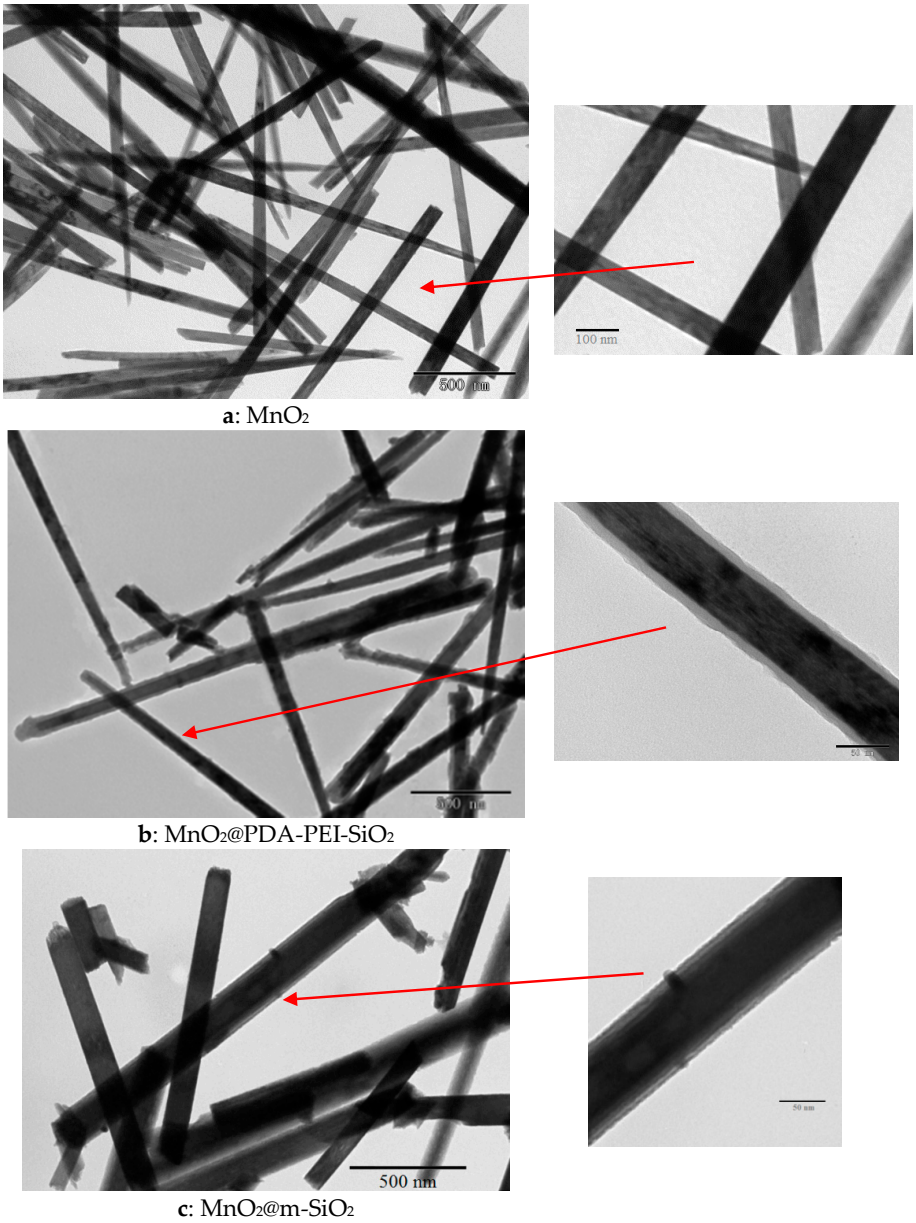

Figure 6. TEM images for MnO_2, MnO_2@PDA-PEI-SiO_2, and MnO_2@m-SiO_2. (**a**) MnO2 nanorods; (**b**) By sequentially coating PDA and PEI and further silicification, a dense film was clearly observed on MnO_2@PDA-PEI-SiO_2; (**b**) The film of PDA-PEI-SiO_2 became mesoporous SiO_2 by removing the PDA-PEI coatings through calcination under 400°C. A tiny gap between the MnO_2 core and the mesoporous SiO_2 shell was generated (**c**).

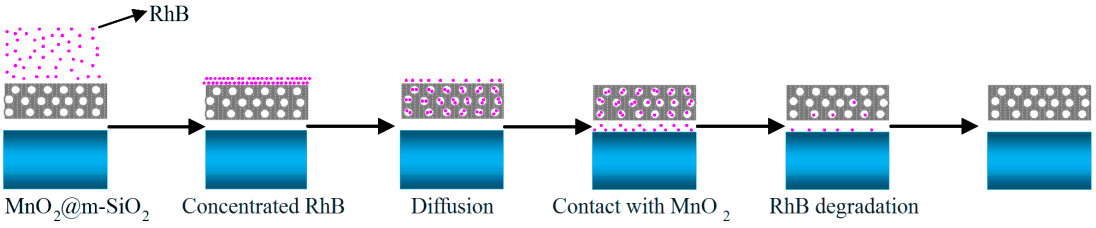

Scheme 2. Schematic presentation of the process for the degradation of RhB using MnO_2@m-SiO_2.

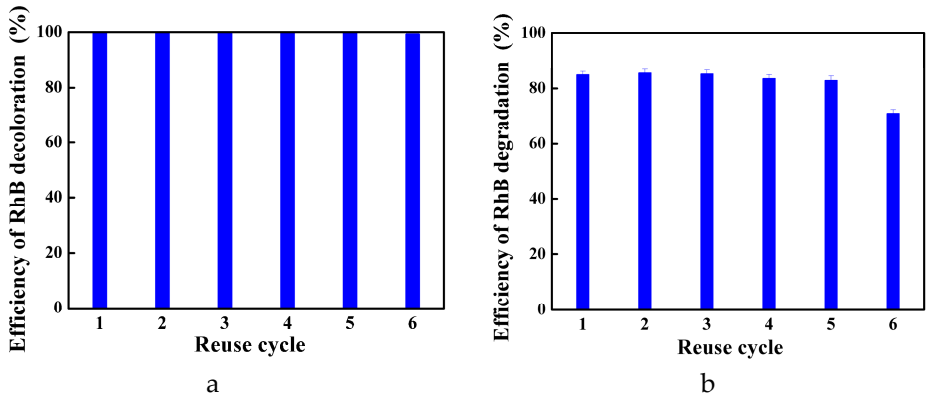

Figure 7. Consecutive use of MnO_2@m-SiO_2 for RhB decoloration (**a**) and degradation (**b**). The immersion time of MnO_2@m-SiO_2 in the solution of RhB was 60 min for each cycle.

3. Experimental Section

3.1. Materials

Dopamine hydrochloride (98%) and PEI were purchased from Sigma-Aldrich (Shanghai, China) and used as received. TEOS, $MnSO_4 \cdot H_2O$, $K_2Cr_2O_7$, and H_2SO_4 were purchased from Sinopharm Chemical Reagent Co. (Shanghai, China). All chemicals are analytical grade or higher, and they were used as received without any further purification.

3.2. Preparation of MnO_2@m-SiO_2 and Synthesis of MnO_2 Nanoroads

For the experiment, 4.056 g of $MnSO_4 \cdot H_2O$ and 2.354 g of $K_2Cr_2O_7$ were mixed in 30 mL double-distilled water. In addition, 3.0 mL H_2SO_4 was then added dropwise under stirring for 30 min. Then, the solution was transferred to a 50 mL Teflon-lined autoclave. The autoclave was sealed and heated in an oven at 120 °C for 12 h. When cooled to room temperature, the resulting brown-black precipitate was collected by filtering through a polycarbonate membrane (0.22 μm), and washed with double-distilled water. MnO_2 nanorods were finally obtained after drying at 80 °C overnight.

3.3. Preparation of MnO_2@PDA

The experiment included 100 mg of MnO_2 nanoroads being added into 100 mL Tris-buffer buffer (pH 8.5) under sonication for 15 min, and then 100 mg dopamine were added. The mixture was sonicated at room temperature for 5 min. The polydopamine-coated MnO_2 nanorods were collected by centrifugation at 8000 g for 10 min, and washed with 30 mL double-distilled water. MnO_2@PDA nanorods were finally obtained after vacuum-freeze drying for 5 h.

3.4. Preparation of MnO_2@PDA-PEI

For the experiment, 50 mg MnO_2@PDA was added to the PEI aqueous solution (25 mL, 2.0 mg/mL). After sonication for 15 min, MnO_2@PDA-PEI was collected by filtering through a 450 nm polycarbonate membrane and then was dried at 80 °C with nitrogen-blowing.

3.5. Preparation of MnO_2@m-SiO_2

A solution consisting of 25 mL water and 5 mL TEOS was prepared. Furthermore, 50 mg MnO_2@PDA-PEI was added to the solution and sonicated at room temperature. After 40 min, the formed MnO_2@PDA-PEI-SiO_2 was collected by filtering through a 450 nm polycarbonate membrane and then was dried at 80 °C with nitrogen-blowing. Then, MnO_2@PDA-PEI-SiO_2 was calcined at 400 °C in air in order to remove PEI and PDA. After 4 h, the formed MnO_2@m-SiO_2 was collected.

3.6. Characterization and Measurement

XPS spectra were measured using an X-ray photoelectron spectrometer (Thermo VG ESCALAB250, Beijing, China). The measurement was carried out at the pressure of 2×10^{-9} Pa. Mg K X-ray was used as the excitation source. UV-Vis spectra were measured on a Shimadzu spectrophotometer (UV2550-PC, Beijing, China). The BET methodology was utilized to calculate the specific surface area. The pore size distribution were derived from the desorption or adsorption branches of isotherms using the BJH model [36].

Infrared spectra were measured using an FTIR spectrometer (Bruker TENSOR 27, Beijing, China). A horizontal temperature-controlled attenuated total reflectance (ATR) with Zn Se Crystal was used. A liquid-nitrogen-cooled mercury-cadmium-telluride detector collected 128 scans per spectrum, and the resolution was 2 cm^{-1}. The ATR element spectrum was used as the background. Ultrapure nitrogen gas was introduced to purge water vapor.

3.7. Catalytic Activity Measurements

MnO_2@m-SiO_2 was used to degrade the model dye RhB. Furthermore, 5 mg MnO_2@m-SiO_2 was added into 10 mL of RhB solution with an initial concentration of 5 mg/mL. The pH was adjusted to be 2.5. MnO_2@m-SiO_2 was well dispersed in the RhB solutions under sonication. After some time, the mixture was centrifuged at 8000 g to separate MnO_2@m-SiO_2 from the solutions. The supernatant was subjected to UV-Vis spectra measurement using a UV-Vis spectrophotometer (UV2550-PC, Beijing, China). In order to explain the degradation process, MnO_2 and MnO_2@PDA-PEI-SiO_2 have also been used to degrade/remove RhB at the same procedures and conditions.

4. Conclusions

A novel core-shell MnO_2@m-SiO_2 has been prepared, consisting of MnO_2 nanorod as the core and mesoporous SiO_2 (m-SiO_2) as the shell. MnO_2@m-SiO_2 has been used to degrade a model dye RhB. The shell m-SiO_2 functions to adsorb/enrich RhB and then to transfer RhB into the tiny gap region between the core and shell, and the core MnO_2 nanorod oxidizes the transferred RhB. The composite MnO_2@m-SiO_2 combines the multiple functions together. Owing to the synergistic effect of the multiple functions, MnO_2@m-SiO_2 has exhibited a much higher efficiency for degradation of RhB than MnO_2. Consecutive use of MnO_2@m-SiO_2 has demonstrated that MnO_2@m-SiO_2 can be used to catalyze multiple cycles of RhB degradation with a good recyclability at ambient temperature.

Acknowledgments: This work was supported by the National Science Foundation of China (21476023).

Author Contributions: Peijun Ji provided the idea and design for the study. Wei Gong, Xianling Meng, and Xiaohong Tang performed the experiments. Wei Gong and Xianling Meng drafted the manuscript, and Peijun Ji revised it.

Conflicts of Interest: The authors declare no conflict of interest.

References

1. Zarei-Chaleshtori, M.; Correa, V.; López, N.; Ramos, M.; Edalatpour, R.; Rondeau, N.; Chianelli, R.R. Synthesis and Evaluation of Porous Semiconductor Hexaniobate Nanotubes for Photolysis of Organic Dyes in Wastewater by. *Catalysts* **2014**, *4*, 346–355. [CrossRef]
2. Junejo, Y.; Sirajuddin; Baykal, A.; Safdar, M.; Balouch, A. A Novel Green Synthesis and Characterization of AgNPs with its Ultra-Rapid Catalytic Reduction of Methyl Green Dye. *Appl. Surf. Sci.* **2014**, *290*, 499–503. [CrossRef]
3. Mallampati, R.; Li, X.; Adin, A.; Valiyaveettil, S. Fruit Peels as Efficient Renewable Adsorbents for Removal of Dissolved Heavy Metals and Dyes from Water. *ACS Sustain. Chem. Eng.* **2015**, *3*, 1117–1124. [CrossRef]
4. Giovannetti, R.; Rommozzi, E.; Anna, C.; Zannotti, M. Kinetic Model for Simultaneous Adsorption/Photodegradation Process of Alizarin Red S in Water Solution by Nano-TiO_2 under Visible Light. *Catalysts* **2016**, *6*, 84. [CrossRef]

5. Liu, X.; Zhang, Q.; Yu, B.; Wu, R.; Mai, J.; Wang, R.; Chen, L.; Yang, S. Preparation of $Fe_3O_4/TiO_2/C$ Nanocomposites and Their Application in Fenton-Like Catalysis for Dye Decoloration. *Catalysts* **2016**, *6*, 146. [CrossRef]
6. Ge, Q.; Wang, P.; Wan, C.; Chung, T.S. Polyelectrolyte-Promoted Forward Osmosis-Membrane Distillation (FO-MD) Hybrid Process for Dye Wastewater Treatment. *Environ. Sci. Technol.* **2012**, *4*, 6236–6243. [CrossRef] [PubMed]
7. Dalui, A.; Thupakula, U.; Khan, A.H.; Ghosh, T.; Satpati, B.; Acharya, S. Mechanism of Versatile Catalytic Activities of Quaternary CuZnFeS Nanocrystals Designed by a Rapid Synthesis Route. *Small* **2015**, *11*, 1829–1839. [CrossRef] [PubMed]
8. Sinha, A.K.; Pradhan, M.; Sarkar, S.; Pal, T. Large-Scale Solid-State Synthesis of Sn-SnO_2 Nanoparticles from Layered SnO by Sunlight: A Material for Dye Degradation in Water by Photocatalytic Reaction. *Environ. Sci. Technol.* **2013**, *47*, 2339–2345. [CrossRef] [PubMed]
9. Teng, F.; Liu, Z.; Zhang, A.; Li, M. Photocatalytic Performances of Ag_3PO_4 Polypods for Degradation of Dye Pollutant under Natural Indoor Weak Light Irradiation. *Environ. Sci. Technol.* **2015**, *49*, 9489–9494. [CrossRef] [PubMed]
10. Cheng, Z.; Liao, J.; He, B.; Zhang, F.; Zhang, F.; Huang, X.; Zhou, L. One-Step Fabrication of Graphene Oxide Enhanced Magnetic Composite Gel for Highly Efficient Dye Adsorption and Catalysis. *ACS Sustain. Chem. Eng.* **2015**, *3*, 1677–1685. [CrossRef]
11. Rampazzo, E.; Bonacchi, S.; Montalti, M.; Prodi, L.; Zaccheroni, N. Self-Organizing Core−Shell Nanostructures: Spontaneous Accumulation of Dye in the Core of Doped Silica Nanoparticles. *J. Am. Chem. Soc.* **2007**, *129*, 14251–14256. [CrossRef] [PubMed]
12. Cohen, B.; Martin, C.; Iyer, S.K.; Wiesner, U.; Douhal, A. Single Dye Molecule Behavior in Fluorescent Core–Shell Silica Nanoparticles. *Chem. Mater.* **2012**, *24*, 361–372. [CrossRef]
13. Feil, F.; Cauda, V.; Bein, T.; Bräuchle, C. Direct Visualization of Dye and Oligonucleotide Diffusion in Silica Filaments with Collinear Mesopores. *Nano Lett.* **2012**, *12*, 1354–1361. [CrossRef] [PubMed]
14. Synak, A.; Bojarski, P.; Grobelna, B.; Kułak, L.; Lewkowicz, A. Determination of Local Dye Concentration in Hybrid Porous Silica Thin Films. *J. Phys. Chem. C* **2013**, *117*, 11385–11392. [CrossRef]
15. Tsai, C.H.; Chang, W.C.; Saikia, D.; Wu, C.E.; Kao, H.M. Functionalization of Cubic Mesoporous Silica SBA-16 with Carboxylic Acid via One-Pot Synthesis Route for Effective Removal of Cationic Dyes. *J. Hazard. Mater.* **2016**, *309*, 236–248. [CrossRef] [PubMed]
16. Deka, J.R.; Liu, C.L.; Wang, T.H.; Chang, W.C.; Kao, H.M. Synthesis of Highly Phosphonic Acid Functionalized Benzene-Bridged Periodic Mesoporous Organosilicas for Use as Efficient Dye Adsorbents. *J. Hazard. Mater.* **2014**, *278*, 539–550. [CrossRef] [PubMed]
17. Wawrzkiewicz, M.; Wiśniewska, M.; Gun'ko, V.M.; Zarko, V.I. Adsorptive Removal of Acid, Reactive and Direct Dyes from Aqueous Solutions and Wastewater Using Mixed Silica–Alumina Oxide. *Powder Technol.* **2014**, *278*, 306–315. [CrossRef]
18. Perullini, M.; Jobbágy, M.; Japas, M.L.; Bilmes, S.A. New Method for the Simultaneous Determination of Diffusion and Adsorption of Dyes in Silica Hydrogels. *J. Colloid Interface Sci.* **2014**, *425*, 91–95. [CrossRef] [PubMed]
19. Kohno, Y.; Haga, E.; Yoda, K.; Shibata, M.; Fukuhara, C.; Tomita, Y. Adsorption Behavior of Natural Anthocyanin Dye on Mesoporous Silica. *J. Phys. Chem. Solids* **2014**, *75*, 48–51. [CrossRef]
20. Malfatti, L.; Kidchob, T.; Aiello, D.; Aiello, R.; Testa, F.; Innocenzi, P. Aggregation States of Rhodamine 6G in Mesostructured Silica Films. *J. Phys. Chem. C* **2008**, *112*, 16225–16230. [CrossRef]
21. Pal, S.; Ghorai, S.; Das, C.; Samrat, S.; Ghosh, A.; Panda, A.B. Carboxymethyl Tamarind-g-poly(acrylamide)/Silica: A High Performance Hybrid Nanocomposite for Adsorption of Methylene Blue Dye. *Ind. Eng. Chem. Res.* **2012**, *51*, 15546–15556. [CrossRef]
22. Valero, D.; Ortiz, J.M.; Expósito, E.; Montiel, V.; Aldaz, A. Electrochemical Wastewater Treatment Directly Powered by Photovoltaic Panels: Electrooxidation of a Dye-Containing Wastewater. *Environ. Sci. Technol.* **2010**, *44*, 5182–5187. [CrossRef] [PubMed]
23. Sarkar, A.K.; Saha, A.; Tarafder, A.; Panda, A.B.; Pal, S. Efficient Removal of Toxic Dyes via Simultaneous Adsorption and Solar Light Driven Photodegradation Using Recyclable Functionalized Amylopectin−TiO_2−Au Nanocomposite. *ACS Sustain. Chem. Eng.* **2016**, *4*, 1679–1688. [CrossRef]

24. Jiao, T.F.; Zhao, H.; Zhou, J.; Zhang, Q.; Luo, X.; Hu, J.; Peng, Q.; Yan, X. Self-Assembly Reduced Graphene Oxide Nanosheet Hydrogel Fabrication by Anchorage of Chitosan/Silver and Its Potential Efficient Application toward Dye Degradation for Wastewater Treatments. *ACS Sustain. Chem. Eng.* **2015**, *3*, 3130–3139. [CrossRef]
25. Remucal, C.K.; Ginder-Vogel, M. A Critical Review of the Reactivity of Manganese Oxides with Organic Contaminants. *Environ. Sci. Prog. Impacts* **2014**, *16*, 1247–1266. [CrossRef] [PubMed]
26. Das, M.; Bhattacharyya, K.G. Oxidation of Rhodamine B in Aqueous Medium in Ambient Conditions with Raw and Acid-Activated MnO_2, NiO, ZnO as Catalysts. *J. Mol. Catal. A Chem.* **2014**, *391*, 121–129. [CrossRef]
27. Ramesh, M.; Nagaraja, H.S.; Rao, M.P.; Anandan, S.; Huang, N.M. Fabrication, Characterization and Catalytic Activity of α-MnO_2 Nanowires for Dye Degradation of Reactive Black 5. *Mater. Lett.* **2016**, *172*, 85–89. [CrossRef]
28. Sun, H.; Xu, K.; Huang, M.; Shang, Y.; She, P.; Yin, S.; Liu, Z. One-Pot Synthesis of Ultrathin Manganese Dioxide Nanosheets and Their Efficient Oxidative Degradation of Rhodamine B. *Appl. Surf. Sci.* **2015**, *357*, 69–73. [CrossRef]
29. Hao, X.; Zhao, J.; Zhao, Y.; Ma, D.; Lu, Y.; Guo, J.; Zeng, Q. Mild Aqueous Synthesis of Urchin-Like MnOx, Hollow Nanostructures and Their Properties for RhB Degradation. *Chem. Eng. J.* **2013**, *229*, 134–143. [CrossRef]
30. Popgeorgievski, O.; Verreault, D.; Diesner, M.O.; Proks, V.; Heissler, S.; Rypáček, F. Nonfouling Poly(ethylene oxide) Layers End-Tethered to Polydopamine. *Langmuir* **2012**, *28*, 14273–14283. [CrossRef] [PubMed]
31. Begum, G.; Rana, R.K.; Singh, S.; Satyanarayana, L. Bioinspired Silicification of Functional Materials: Fluorescent Monodisperse Mesostructure Silica Nanospheres. *Chem. Mater.* **2010**, *22*, 551–556. [CrossRef]
32. Zangmeister, R.A.; Morris, T.A.; Tarlov, M.J. Characterization of Polydopamine Thin Films Deposited at Short Times by Autoxidation of Dopamine. *Langmuir* **2013**, *29*, 8619–8628. [CrossRef] [PubMed]
33. Gasnier, A.; Pedano, M.L.; Gutierrez, F.; Labbé, P.; Rivas, G.A.; Rubianes, M.D. Glassy Carbon Electrodes Modified with a Dispersion of Multi-Wall Carbon Nanotubes in Dopamine-Functionalized Polyethylenimine: Characterization and Analytical Applications for Nicotinamide Adenine Dinucleotide Quantification. *Electrochim. Acta* **2012**, *71*, 73–81. [CrossRef]
34. Silverstein, R.; Bassler, G.; Morrill, R. *Spectrometric Identification of Organic Compounds*; John Wiley & Sons: New York, NY, USA, 1981.
35. Briggs, D.; Seah, M.P. *Practical Surface Analysis*, 2nd ed.; John Willey & Sons: New York, NY, USA, 1993; Volume 1.
36. Barrett, E.P.; Joyner, L.G.; Halenda, P.P. The Determination of Pore Volume and Area Distributions in Porous Substances. I. Computations from Nitrogen Isotherms. *J. Am. Chem. Soc.* **1951**, *73*, 373–380. [CrossRef]
37. Daneshvar, N.; Behnajady, M.A.; Mohammadi, M.K.A.; Dorraji, M.S.S. UV/H_2O_2 Treatment of Rhodamine B in Aqueous Solution: Influence of Operational Parameters and Kinetic Modeling. *Desalination* **2008**, *230*, 16–26. [CrossRef]